J. Am. Soc. Mass Spectrom. (2019) 30:905–918
DOI: 10.1007/s13361-019-02184-9

FOCUS: ION MOBILITY SPECTROMETRY (IMS): RESEARCH ARTICLE

Determination of Gas-Phase Ion Structures of Locally Polar Homopolymers Through High-Resolution Ion Mobility Spectrometry–Mass Spectrometry

Xi Chen,[1,2] Shannon A. Raab,[3] Timothy Poe,[1] David E. Clemmer,[3] Carlos Larriba-Andaluz[1]

[1]Department of Mechanical Engineering, IUPUI, 723 W Michigan st, Indianapolis, IN 46202, USA
[2]Department of Mechanical Engineering, Purdue Universiy, West Lafayette, IN 47907, USA
[3]Department of Chemistry, Indiana University, 800 E Kirkwood Ave, Bloomington, IN 47405, USA

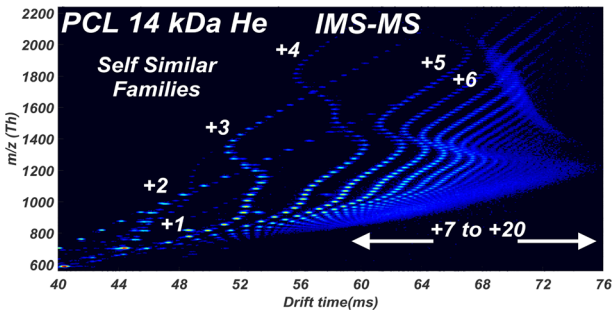

Abstract. The strong synergy arising from coupling two orthogonal analytical techniques such as ion mobility and mass spectrometry can be used to separate complex mixtures and determine structural information of analytes in the gas phase. A tandem study is performed using two systems with different gases and pressures to ascertain gas-phase conformations of homopolymer ions. Aside from spherical and stretched configurations, intermediate configurations formed by a multiply charged globule and a "bead-on-a-string" appendix are confirmed for polyethylene-glycol (PEG), polycaprolactone (PCL), and polydimethylsiloxane (PDMS). These intermediate configurations are shown to be ubiquitous for all charge states and masses present. For each charge state, configurations evolve in two distinctive patterns: an *inverse* evolution which occurs as an elementary charge attached to the polymer leaves the larger globule and incorporates itself into the appendage, and a *forward* evolution which reduces the globule without relinquishing a charge while leaving the appendix relatively constant. *Forward* evolutions are confirmed to form self-similar family shapes that transcend charge states for all polymers. Identical structural changes occur at the same mass over charge regardless of the system, gas or pressure strongly suggesting that conformations are only contingent on number of charges and chain length, and start arranging once the ion is at least partially ejected from the droplet, supporting a charge extrusion mechanism. Configurational changes are smoother for PDMS which is attributed to the larger steric hindrance caused by protruding pendant groups. This study has implications in the study of the configurational space of more complex homopolymers and heteropolymers.

Keywords: Ion Mobility Spectrometry, IMS, polymer, PEG, PCL, PDMS, Homopolymer, Mass Spectrometry, IMS-MS, drift tube, DMA, Structure, Polyethylene-glycol, Polycaprolactone, Polydimethylsiloxane

Received: 12 January 2019/Revised: 18 February 2019/Accepted: 5 March 2019/Published Online: 16 April 2019

Introduction

Synthetic and natural polymers play an essential role in modern day life across all different disciplines and industries (e.g., biological, chemical, pharmaceutical, additive manufacturing, industrial, etc.) [1–5]. Their interest resides in their large variety in composition, structure, molecular weight, and their distinct and unique physical properties [6, 7]. Indeed, global production of synthetic polymers has reached 300

Xi Chen and Shannon A. Raab have contributed equally to this work

Electronic supplementary material The online version of this article (https://doi.org/10.1007/s13361-019-02184-9) contains supplementary material, which is available to authorized users.

Correspondence to: Carlos Larriba–Andaluz; *e-mail:* clarriba@iupui.edu

million tons and is expected to double in the next 10 to 15 years [8]. In the biological context, all organic macromolecules such as nucleic acids, proteins, and polysaccharides are polymers with fundamental functional roles where structure is a key component [9, 10]. As more advanced manufacturing techniques surface and better understanding of biological processes arise [11], polymers are bound to become the building blocks of synthetic and natural molecular motors [12], will have important roles in information processing at the nano-level and may give rise to intricate self-assembled nano-objects [13–16]. A deeper understanding of polymers as single physical objects is however crucial for these promising applications to materialize.

In recent years, techniques such as single-molecule spectroscopy and optical tweezers have allowed us to control biological macromolecules as single entities, where folding or misfolding may be studied and imitated with synthetic counterparts [17–20]. Important advances in mass spectrometry (MS) have also allowed polymers to be uniquely characterized individually [21–24]. When MS is coupled with orthogonal techniques such as ion mobility spectrometry (IMS), a new dimension is brought forth that also yields insight into the gas-phase structures of these ions. When used in conjunction with electrospray ionization (ESI), ESI-IMS-MS has provided valuable structural information of polymers in the gas phase [25]. Most notable are the studies of the hydrophilic homopolymer polyethylene glycol (PEG), whose very simple backbone structure and ability to hold positive charge (through its oxygen sites) has led to some of the most revealing spectra in the field of ion mobility.

Initial work by Fenn and colleagues on PEG using MS showed that even with mean molecular weights in the range of megadaltons, the highest intensity of the spectra appeared to be at around 900 Thomsons (Th), suggesting that the ions were heavily charged and that the vast majority of the ions would have to be stretched to contain such amount of charge [26–29]. Von Helden, Wyttenbach, and Bowers showed using different mechanisms, including IMS-MS and molecular dynamics (MD), that charges in the ion are surrounded by the polymer chain, as if it were solvated, in what was referred to (perhaps later on) as a "beads-on-string" configuration [30–33]. The number of monomer linkers surrounding the charge (coordination number) varied between 6 and 12 depending on the polymer used (around 8 for the sodiated PEG structures observed). They were equally successful in showing that more compact globular PEG ions must exist when the level of charging is low enough. Ude and de la Mora combined a differential mobility analyzer (DMA) together with an MS to show that "intermediate" structures were present, between fully globular and stretched, which were uniquely defined for each charge state [34]. Moreover, they hinted at the existence of non-spherical shape families that transcended a single charge state (the same shape was observed in multiple charge states). Trimpin, Clemmer, and coworkers used high-resolution IMS-MS with PEG and other polymers to show that uniquely defined intermediate shapes were present joining the spherical/globular region with the stretched one by a series of sharp kinks attributed to collapsing transitions [35, 36]. MD simulations of longer multiply charged chains revealed extended structures confirming the "beads-on-string" configuration for ions with a degree of polymerization (DP) of 126 and 9 charges [35, 36]. Within our group, a differential mobility analyzer mass spectrometer (DMA-MS) was used to characterize the full extent of these transitions for the first 8 charge states with multiple incomplete transitions for higher charge states [37]. Careful study of the mobilities revealed that the transition structures may be precisely determined and that the configurations created are heavily dependent on the number of charges and the length of the chain. MD simulations, as well as analytical and numerical collision cross section (CCS) predictions showed that the existing structures were formed by a multiply charged globule with a "beads-on-string" appendix sticking out and where the equilibrium is established by the competition between cohesive forces (Van der Waals) and repulsion between charges [38, 39]. Our group also confirmed the existence of these self-similar shapes predicted by Ude et al., established their structure, and extended their presence to all visible structures and charge states in the spectra up to 8 kDa [37].

The fact that the observed mobility peaks were so sharply defined in both mobility and mass, in contrast to what occurs for example for large proteins where mobility peaks are in general broader than the limit of resolution of the instrument, led to the belief that the ions are at least partially produced by the ion evaporation model (IEM) from the ESI droplet instead of through the more common charge residue model (CRM) for large ions [40–42]. This has been corroborated independently by Konermann et al. and Consta et al. through MD simulations and whereby a macromolecule is extruded from a charged droplet attached to the ejected charges in a sequential fashion. Konermann first showed that this effect is applicable to proteins in what has been termed as the chain ejection model (CEM) [43, 44]. Recently, he has shown that the CEM mechanism applies partially to polypropylene glycol polymers as well [45]. Consta, on the other hand, provided simulations of the release mechanisms of PEG and an analytical model for the extrusion of a chain from a droplet [46, 47]. For simplification purposes, we will refer to the release, ejection or extrusion of a chain as chain extrusion, leaving the intricacies of the differences between the methods to more detailed literature [48, 49]. Our group partially confirmed the reality of the chain extrusion process through gas-phase ion activation of two entangled polymer molecules in the gas phase in an IMS-IMS cell [50]. When sufficient energy was applied, the chains were disentangled in the gas phase and each individual chain instantly rearranged itself onto different configurations depending on the number of charges and the number of monomers in each chain. What is more important, these configurations agreed with the configurations arising from the solution droplet. The ability of the polymer to ion evaporate from a polymer melt in the gas phase and reconfigure itself into a configuration resembling that extruding from a droplet is, in our opinion, clear evidence that charge extrusion and restructuring in the gas phase is a natural behavior for polymer ionization.

More recently, de Pauw's group has been working on a thorough study of polymer topology using IMS-MS where they use the concept of apparent densities to establish relations between mass and CCS [51–53]. Many of the implications of the topological study of homopolymers in the gas phase can and should be used to explain some of the behaviors observed in more complex heteropolymers, e.g., nucleic acids and proteins. It has become clear that CCS of proteins in the gas phase are not limited to the biologically more relevant functional form or native state, but rather depend on many other external parameters. Many times, the major contributor to protein deformation in the gas phase is the level of charge, particularly under denaturing conditions where the protein appears extended. However, compaction in the gas phase when the level of charge is relatively low has also been observed for proteins like cytochrome C, immunoglobulins, or even viruses [54–63]. This complexity is enhanced by the details of how the ions are handled prior to mobility measurements, including the conditions in the solvent, the ionization process, or the pressure changes in the interface. All these effects yield different configurations, especially under denaturing conditions, that must be interpreted in order to correctly answer the most pressing issue; which, if any, of the gas-phase configurations corresponds to the native structure of the protein?

To further explore and understand the gas-phase structures of homopolymers and heteropolymers, this manuscript explores the concept of local monomer polarity in homopolymers to extend the structural configurations already observed in PEG to other polymers such as polycaprolactone (PCL) and polydimethylsiloxane (PDMS). The idea herein is that the oxygen (electronegative) sites present in the PCL and PDMS monomers, as shown in Figure 1, is sufficient to bind the polymers to the charging agent (in this case ammonium) despite the overall molecule being somewhat non-polar (non-miscible in water). A feature of the structures must therefore be the flexibility of the polymer to wrap around the charge together with the enhanced attraction produced by the existing polar bond. PCL and PDMS were also chosen because both present discernable differences with respect to PEG. PCL is intrinsically very similar to PEG with a very simple backbone chain and a single oxygen as a pendant group, but where the monomer is almost three times the mass of the PEG monomer, increasing the mass over charge gap between consecutive ions. The carbon to oxygen ratio has also been increased from 2 to 1 for PEG to 5 to 2 for PCL which has implications in the monomer coordination number. On the other hand, PDMS has an organosilicon based backbone with a monomer molecular mass between that of PEG and PCL. PDMS, however, has two methyl pendant groups that shield the heavily polarized backbone. These pendant groups also reduce the flexibility of the chain and contribute to the transitions occurring at larger masses and lower mobilities.

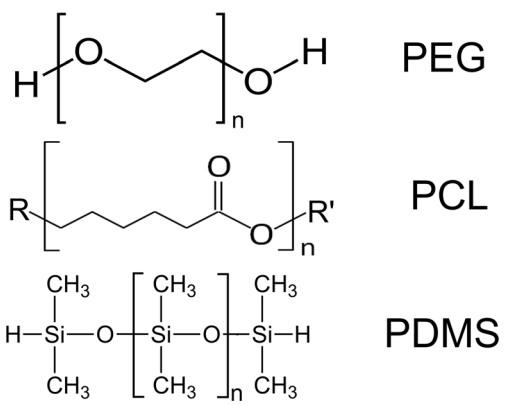

Figure 1. Sketches of polymers

The studies of these three polymers are made using two very different IMS-MS systems and conditions albeit with the similarity that the mobilities calculated in both systems are directly related to the raw variables used. The first system is an ultra-high resolution (R~150–400) 4 m drift tube that operates at low pressure and He gas coupled to an in-house MS system. The second system is a high resolution (R~50–60) DMA system that operates at atmospheric pressure in N_2 coupled to a commercial triple–quadrupole time of flight system (ToF). Both systems use similar ESI sources to ionize the same analyte solutions in order to lower the amount of external variables that might affect the gas-phase configurations. It is shown that the gas-phase structures are independent of the buffer gas and pressure used (at least in the range studied) and that the different transitional changes in each of the polymers seem to appear at the same mass over charge for either experimental system. The high resolution achieved with the drift tube allows many of the transitions to be completely resolved clearly for the first time where charge states "interweave." These transitions seem to extend to very high charge states and masses (up to the resolving power of the instrument and up to hundreds of kDa) without any observable difference in the family self-similar shapes. As such, the globule plus appendix structures present in PEG are confirmed for the other two polymers. Moreover, the transitions for PCL appear to be analogous to those of PEG while PDMS follows similar trends but with less sharp transitions. This is to be expected due to the increased steric hindrance caused by the methyl pendant groups.

Experimental Setups and Methods

Two experimental systems were used to obtain the results presented in this manuscript. The first one is an atmospheric pressure Differential Mobility Analyzer (SEADM, P4, Boecillo Spain, R~50–60) coupled to a triple–quadruple time-of-flight (ToF) mass spectrometer (QSTAR XL, R~10,000) [64]. The second system corresponds to a homemade 4-m low-pressure drift tube (R~150–400) coupled to a ToF system (DT-MS). Both systems, each with their own electrospray emitter, are described below.

Differential Mobility Analyzer Mass Spectrometer (DMA-MS)

The operation of the DMA has been shown previously, and only a brief explanation will be provided here [65]. The DMA is, as its name suggests, a filter that transmits a single ion mobility (within the instrument's resolution) under a specified condition. For the parallel plate DMA used in this work, see Figure 2A, mobility classification may be achieved by applying a voltage difference between two parallel plates while a sheathed gas (nitrogen) flows between these plates at a constant velocity. Ions entering a slit on the top electrode will be pushed downstream by the sheathed gas while drifting towards the bottom electrode due to the electric field. This combination of voltage and gas flow spreads the ions spatially depending on their mobility. An outlet slit placed on the bottom electrode 4 cm downstream of the inlet slit allows ions of a particular mobility to drift into the QSTAR MS which operates in RF mode only. Varying the voltage will modify the ion mobility that is transmitted into the MS. The desired mobility is easily obtained from the voltage through the linear equation:

$$K_{DMA} = k/V_{DMA} \tag{1}$$

where K_{DMA} is the ion mobility, V_{DMA} is the DMA voltage applied, and k is a value proportional to the distance between electrodes, the distance between slits, and to the velocity of the gas flow. Due to the difficulty in accurately calculating the flow velocity, k is normally obtained through calibration. In this manuscript, THA^+ ion was used to calibrate the spectra ($K_{cal} = 0.984$ cm^2/Vs at room temperature and pressure) [66]. An IMS-MS scan and spectra are therefore produced by ramping the voltage (at steps of a few volts every second) within a range of desired mobilities. Some of the advantages of the DMA are that it is able to work at atmospheric pressure, that its integration with any existing MS can be done very easily, that it allows only a single mobility into the MS, and that its mobility is easy to relate to the raw variables employed. While the base resolution of the DMA is set at 50–60, one can obtain resolutions larger than 110 [67]. In fact, some of the resolutions observed in this manuscript for large charge states is above 175.

ESI Electrospray for DMA-MS

In order to electrospray the polymer ions, samples were introduced into a 1.5-mL polypropylene vial, which was pressurized above atmosphere to push the solution through a silica capillary (Polymicro Technologies, ID 41 μm, OD 360 μm). The silica was tapered at the tip to ease the anchoring of the meniscus. An HV floating power supply (EMCO HV Co., Sutter Creek, CA) is then used to apply a voltage between the liquid reservoir and the top electrode producing a Taylor Cone and a microdroplet jet. The Taylor Cone was monitored through a camera until it was visually stable and produced a constant current of 70–180 nA measured with a multimeter. The capillary was then centered and placed 0–2 mm away from the DMA slit so that ions were not lost in the spread. A small counterflow (0–0.4 lpm) of nitrogen (similar to a curtain gas) was employed to ensure any neutrals from entering the system while enhancing the solvent evaporation.

Drift Tube Mass Spectrometer IMS-MS (DT-MS)

A home-built 4-m drift tube coupled to a ToF mass spectrometer was used for DT-MS analysis. A description of drift tube theory of similar instrumentation has been given in detail previously [68, 69], and only a brief description is provided here together with the sketch shown in Figure 2B. Ions produced by ESI enter the IMS-MS instrument through a narrow capillary and are stored in an hourglass-shaped ion funnel. A 100-μs-wide electrostatic gate is used to pulse the ions into the drift tube at specified intervals. The ion packet then traverses the drift region under the influence of a uniform electric field (11.5 V cm^{-1}) and is free to collide with a neutral buffer gas (~ 3.0 Torr He). After every meter of separation, the diffuse ion packet is radially focused by ion funnels with applied RF potentials (F# in the figure). When the ions exit the drift tube through a differentially pumped region, they are pulsed into a two-stage reflection-geometry ToF-MS and separated by their mass-to-charge ratios (m/z). The corresponding drift times and flight times are detected by a microchannel plate and are recorded in a nested fashion [70]. The conversion from drift time to mobility, K_{DT}, is hence given by:

$$K_{DT} = k'/t_{drift}. \tag{2}$$

Here, k' is a constant (length divided by electric field) that establishes the relation between mobility and drift time. In a similar fashion to the DMA, k' is not directly calculated and a calibrant is used to obtain the mobility. In this work, the doubly charged Bradykinin ion (m/z ~530 Th, CCS~246A^2) is used to calibrate the spectra.

ESI Emitter Fabrication for DT-MS

Uncoated borosilicate glass (ID 1.2 mm, OD 1.5 mm) was purchased from Sutter Instrument Co. (Novato, CA). The 10-cm-long capillaries were pulled with a Sutter P-97 micropipette puller to produce electrospray capillaries with 10-μm tip sizes and taper lengths of ~4 mm. These tips have been well characterized previously by scanning electron microscopy to ensure reproducibility. The polymer solution was inserted into the back of a pulled emitter, and a 0.25-mm platinum wire was inserted into the solution. The emitter was positioned onto a stage for alignment to the IMS-MS instrument. An ESI potential between 1 and 2 kV (Bertan, Spellman High Voltage, Hauppauge, NY, USA) was connected to the platinum wire to generate ions for analysis.

Analytes

Solutions of micromolar concentrations of polymer in different solvents with varying levels of ammonium acetate

(AmAc, Sigma-Aldrich, St Louis, MO) were used. Polyethylene glycol 12 kDa (Sigma-Aldrich), at concentrations of 300 μM, was dissolved in a 50/50 water-methanol (UPLC-grade, Sigma-Aldrich) mixture with the addition of 10–30 mM AmAc. Due to the non-solubility of PCL and PDMS in water, toluene (Sigma-Aldrich) was used for the other polymers. One hundred to 300 μM poly-caprolactone 14 kDa (Sigma-Aldrich) was dissolved in a 50/50 toluene-methanol with concentrations of 10–70 mM AmAc salt. Concentrations of 100–300 μM of PDMS 25 kDa (1150 cSt, Sigma-Aldrich) in a 50/50 solution of toluene and methanol with 30 mM of AmAc. The densities used for the polymers are 1115 kg/m^3 for PEG [71], 1145 kg/m^3 for PCL [72], and 965 kg/m^3 for PDMS [73].

Calculations of CCS

In order to relate the mobility of the ions to their CCS in the gas phase, one can make use of the well-known Mason–Schamp equation for small ions in the free molecular regime [74]:

$$K = \frac{3}{16}\frac{ze}{N}\left(\frac{1}{m}+\frac{1}{M}\right)^{\frac{1}{2}}\sqrt{\frac{2\pi}{k_bT}}\frac{1}{\Omega_{gas}} \quad (3)$$

Here, z is the integer charge number, e is the elementary charge, k_b is the Boltzmann constant, T is the temperature, N is the gas density, m and M are the molecular mass of the gas and the ion (respectively), and Ω_{gas} is the CCS of the ion which depends on the buffer gas used. The raw variable DMA-MS voltage may be transformed into mobility by use of the calibrant ion data. This mobility, in turn, is transformed into CCS through Eq. (3). If mobilities are preferred, the CCS obtained with the calibrant data from the DT-MS could in turn be transformed into mobility.

Results and Discussion

To explore the reasons why homopolymers seem to arrange themselves in well-defined structures in the gas phase, polymers with very distinct monomer units were used in conjunction with different IMS-MS systems working at different conditions of pressures in different gases.

The homopolymers, PEG, PCL, and PDMS, were carefully chosen for this study for their unique similarities and differences, with their backbone chains sketched in Figure 1. A shared characteristic of these polymers is that the monomer unit possesses some local electronegativity so that the positive charging agent employed can easily attach to the site and allow the polymer to hold a vast amount of charge. While completely non-polar polymers, e.g., polypropylene, will never hold sufficient charge to become stretched in the gas phase, it is also not necessary for the polymer to be globally polar or hydrophilic. As such, even though PEG is soluble in water, the other two polymers are not despite having polar covalent bonds. In the case of PDMS, the non-polar methyl groups shield the backbone of the structure yielding it non-soluble in water. PCL is known for its hydrophobicity and as such can only be dissolved in non-polar solvents such as toluene. Despite this, PCL has a local polar region (see sketch) which is not shielded and where positive charge can easily attach.

The monomer unit masses of 44 Da for PEG, 74 Da for PDMS, and 114 Da for PCL will give a reasonable range of monomer molecular masses to compare. The mean molecular weights of the polymers are 12 kDa, 25 kDa, and 14 kDa, and the distributions are very broad, so it is expected that masses ranging from a few hundred to tens of thousands of Daltons may be observable in the mobility-mass spectra.

The addition of AmAc salt increases the conductivity of the sample while allowing ammonium ions to attach themselves to the polymer chains. Even though other charging agents may work as well, AmAc is specifically chosen in this case for its ability to attach to the polymer sites strongly. While not shown here, AmAc produces the least number of evaporation events (loss of charge in the IMS or MS regions) when compared to other charging agents. It seems that the hydrogen in the ammonia ion enhances the ability of the charge to stick to the polymers' oxygen sites, in comparison to for example Na^+, especially in the air to vacuum interface and in particular when declustering potentials are used [50]. If the charging agent was to be negative, then very few charges should attach to the chain. As expected, electrospraying PEG in negative mode only yields globular ions [75].

IMS-MS Studies under N_2 and He Gases

To study the effect of different gases on the structural configuration of the polymers, two distinct systems have been used. A DMA-MS which works in N_2 at atmospheric pressure and a DT-MS which works in He at low pressure (~3 Torr). The systems are different enough that the similarities between the two results might give insight into the generalization of the gas-phase configurations produced. Both systems are also alike in the sense that mobility is inversely proportional to the raw data variable in the abscissa axis, be it drift time or DMA voltage, making the interpretation and comparison easier. All three polymers were run under both systems and the results are shown in Figure 3. Figure 3 contains six color scheme contour plots where the ordinate axis corresponds to mass over charge in Thomsons and the abscissa axis corresponds to the raw variable pertaining to the particular system (drift time or DMA voltage). The false color scheme determines the intensity which is only representative of the signal that arrives at the detector but is not guaranteed to relate to the real mass distribution of the polymer ions. Figure 3a, b shows PEG 12 kDa under He (a) and N_2 (b) environments, Figure 3c, d shows PCL 14 kDa under He and N_2, respectively, and finally, Figure 3e, f shows PDMS 25 kDa for the same two gases. Clean full-resolution one-page images of each of the plots are provided in the Supplementary Information.

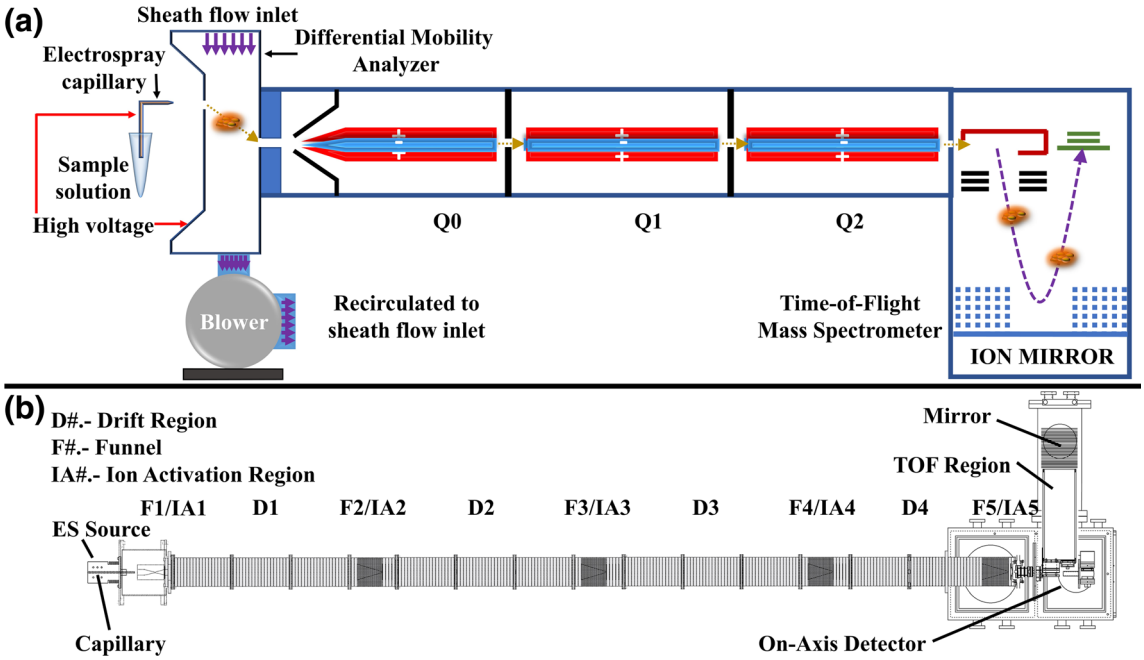

Figure 2. Experimental sketches of (**a**) DMA-MS and (**b**) DT-MS

Particularities of Contour Plots

The ionic spectra produced are quite similar regardless of the polymer or gas used and certain parallelisms can be made for all plots. Some of the features have already been described previously for PEG, and only a brief explanation of those is provided here [37, 39, 50]. Since the homopolymer mass distributions are quite broad, the plots are populated by a myriad of ions which correspond to different chain lengths (different DP) centered, in general, on the mean molecular weight of the polymer. These chains may also have varying amounts of charge for the same length which ultimately leads to the wide spectra observed. The fact that the jump between two ions differing one monomer link is constant in mass over charge, *m*/*z*, leads to distinct *tracks* in the plots which are easily discernable and correspond to constant charge states labeled +z. Depending on the degree of polymerization, the chains arrange themselves in different structures within the *tracks*. For each *track*, three regions are readily observable: (1) the heavily charged fully stretched region at low *m*/*z* and high mobilities, (2) the low-charge globular (spherical) region at small mobilities and medium to high *m*/*z* (see Figure 3b showing the globular region for charge state 4), and (3) a set of transition regions with multiple kinks joining the globular region to the stretched region.

Before describing each individual polymer plot in detail, the highly resolved plots provided by the DT will easily provide a more in-depth explanation of the *tracks* and transitions. PEG spectra in He may be used for this purpose as shown in Figure 4. Figure 4a provides a guide to *tracks* + 5 through + 8 as they intertwine through the various kinks from globular to stretched as *m*/*z* is lowered. While *tracks* + 1 through + 7 are complete, tracks + 8 through + 13 can be followed for some or most of the *track* (up to the highest *m*/*z* observable by the MS). Higher charge states are also visible, but the *tracks* are incomplete and only appear partially in regions corresponding to the mean molecular weight of the polymer.

To understand how the polymer ions arrange themselves into different structural configurations in the transition regions, Figure 4b describes the process for *track* + 4. To describe this process, ions are assumed to have entropically driven configurations in the solvent before it is electrosprayed into a plume of droplets. Inside the droplets, or perhaps at the surface, the polymer wraps around the ammonia charges with a coordination number between 8 and 12. As the solvent evaporates, the beads are ion-evaporated from the droplet one at a time (chain extrusion) and conform their structure mid-flight in the gas phase. This sequence of ion evaporation events has been gaining more acceptance and has been described extensively through molecular dynamic simulations [44–46, 48, 49, 76]. It also seems to agree with the data presented here for reasons described herein. One of such reasons is the remarkable resolution of the peaks in both mobility and *m*/*z*. In general, in Dole's charge residue mechanism [41], impurities remaining in the droplet with the ion are known to appear in the IMS-MS spectra which lower resolution in mass and mobility, something not observed here. It is however almost certain that some of the largest globular ions with low charge that appear in this work must occur through Dole's mechanism.

Once in the gas phase after the ion ejection, the polymer arranges itself into a particular configuration depending on the number of charges and the length of the chain [37]. An ion with a high degree of polymerization (for PEG + 4, DP > 182, *m*/*z* > 2000) that desorbs with 4 charges will have enough cohesive force to withstand the existing repulsive forces and become globular. This is represented by letter A in Figure 4b. When an ion with 4 charges has a degree of polymerization below the

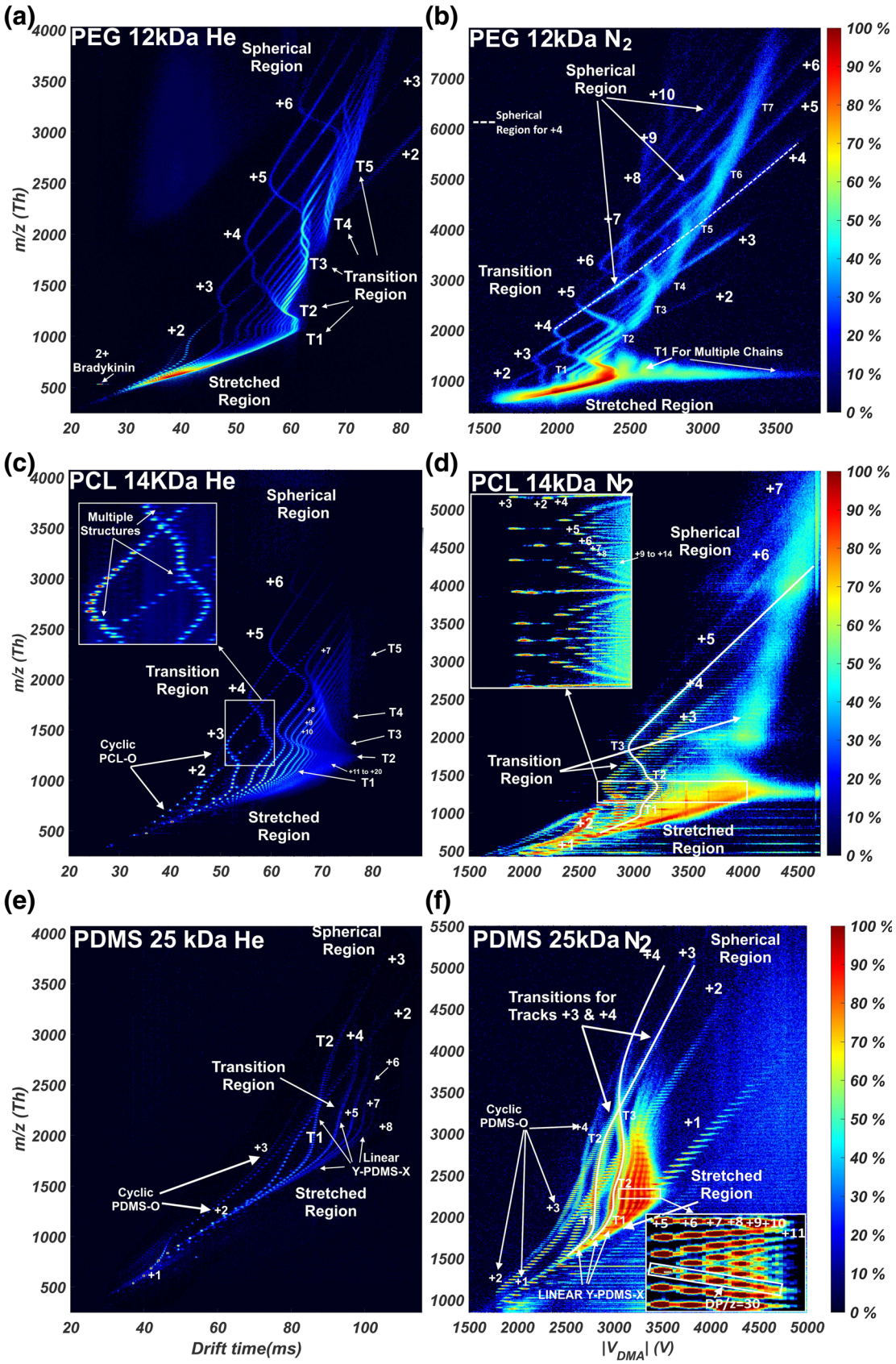

Figure 3. Contour plots of polymer spectra in He and N_2 conditions. (**a**) PEG 12 kDa He, (**b**) PEG 12 kDa N_2, (**c**) PCL 14 kDa He, (**d**) PCL 14 kDa N_2, (**e**) PDMS 25 kDa He, (**f**) PDMS 25 kDa N_2

first critical value but above a second critical value (for PEG + 4, 145 < DP < 182, 1600 < *m*/*z* < 2000), the ion will no longer be able to overcome the repulsive forces completely. It will however try to find its most stable configuration—a local minimum—in the gas phase [34, 39]. This has been observed to be a globule with *z*-1 charges with a single bead appendix sticking out and which corresponds to letter B in Figure 4b [37]. In this transition region, between 1600 and 2000 *m*/*z*, there are two distinct ion mobility tendencies. The first one corresponds to an increase in CCS (decrease in mobility) as the *m*/*z* is lowered, while the second one corresponds to a decrease in CCS (increase in mobility) with decreasing *m*/*z*. The only possible scenario for these two sharp tendencies to occur is that two different restructuring processes occur mostly independent of each other. In the first process, termed from here on *inverse* evolution (from *m*/*z* of 2000 to 1700–1750 Th for PEG + 4), chains with subsequently lower DP will reconfigure themselves so that the appendix becomes longer at the expense of losing monomers in the globule. The continuous extension of this appendix greatly increases the CCS and significantly lowers the mobility as the DP is lowered through the *track*. Somewhere in the 1700–1750 Th, the appendix reaches sufficient length so that the repulsion is small enough and the appendix stops growing.

At this point, the second process starts—termed *forward* evolution—and covers in PEG + 4 a reduction in the DP from 1750 to 1600 Th. The reduction of DP seems to only affect the size of the globule with the remaining charges ($z = 3$) keeping the appendix length constant and thus the trend is reversed (CCS lowers with mass). This reduction of the globule continues until the repulsion in the globule is strong enough that the ion cannot group all three charges together and a second appendix is produced, which is normally an extension of the first (100 < DP < 145). As such, a second transition occurs from 1600 to 1100 Th with the same characteristics as the first. In here, from around 1600 to 1400 Th, the second appendix protrudes in the *inverse* evolution portion while from 1400 to 1100 Th (C in Figure 4b), the globule with the remaining 2 charges is reduced in the *forward* evolution (to letter D in Figure 4b). When the ion's DP is small enough (DP < 100), there are not sufficient monomers to group two charges in a single globule and the ion remains fully stretched with perhaps a slightly larger singly charged globule (E in Figure 4b).

These sets of transitions, each with a *forward* and *inverse* evolution, occur in the same fashion for all existing *tracks* (and all the polymers studied here) as shown in Figure 4a, which finally lead to the interweaved patterns observed in the plots. Each track has no more than *z*-1 transitions from globular to fully stretched. The transitions are labeled by TX, where X is an integer number from 1 to *z*-1 and where T1 refers to the transition closer to the stretched region (as observed in Figure 3). In higher charge states (+ 5 or greater), some of the last transitions (into the globular region) are skipped probably due to the fact that the repulsive-cohesive equilibrium length for the last remaining portion of the appendix does not seem to be reached before a new charge must leave the globule.

Particularities of the PEG Spectra

While the PEG ion has been explored extensively before as shown in the introduction, it has not been done with the detail of resolution provided here. The high resolution of the DT-MS

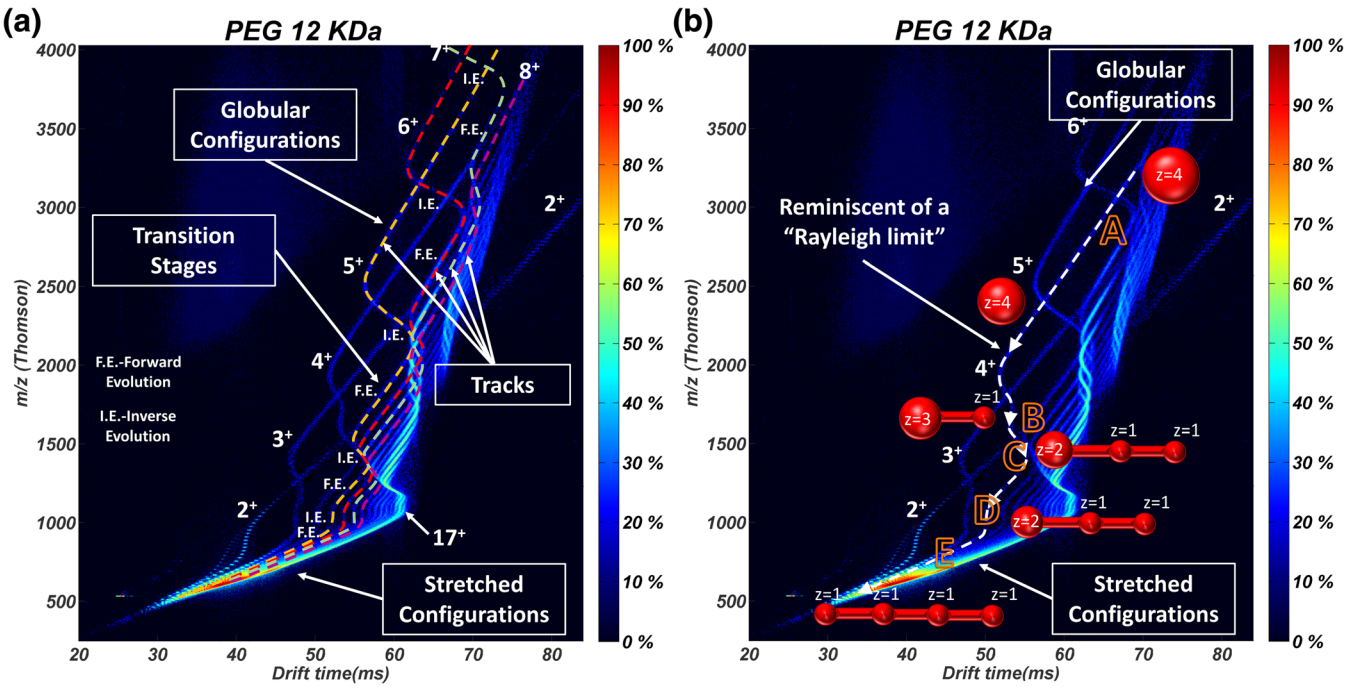

Figure 4. (**a**) PEG contour plot highlighting different charge state tracks as well as inverse and forward evolutions. (**b**) PEG contour plot showing the evolution of the structures for track +4 from globular to stretched. Letters correspond to the different structures sketched

in He allows the first four (starting from the stretched side) transitions to be fully discernable for a multitude of charge state *tracks* as they interweave each other during the *inverse* evolutions. This will allow a more thorough comparison of the CCS for each *track* and transition. Each of these transitions have been labeled in Figure 3a as T1 through T4, with T5 also slightly visible. The TX label is also followed by an arrow that points at the *inverse* evolution portion. Some general rules seem to be present for different tracks within the same transition; for example, *inverse* and *forward* evolutions seem to follow similar patterns as if mimicking each other. One *inverse* evolution that stands out is that of T1 which seems to be weaker than that of other transitions to the point that the CCS remains almost constant (instead of increasing) when lowering the mass over charge.

The N_2 plot, Figure 3b, repeats the same spectra as the He plot albeit with lower mobility resolution. The MS used however has a higher *m*/*z* resolution and reaches much higher *m*/*z*. For this reason, higher globular charge states as well as higher transitions are observable. As shown previously, these larger *m*/*z* correspond to more than one polymer chain entangled together [50]. It also seems that the multiple blobs appearing at $m/z = 1200$ Th and $V_{DMA} > 2500$, not observed in He, seem to be the first transition, T1, of subsequent entangled chains (labeled "T1 for multiple chains" in the figure). This is supported by the fact that these blobs of multiple linked chains do not continue into the stretched regions as subsequently lower cohesive forces and stronger repulsive ones would most likely disentangle the chains (there is no *m*/*z* below 1000 for any of these blobs).

One interesting feature that stands out when comparing both PEG plots is that the kinks and transitions all happen at the same *m*/*z* for both gases, N_2 and He, which seems to suggest that the structures formed in the gas phase are not strongly dependent on the gas or the pressure. This also implies that the gas-phase structures are mostly a function of potential interactions confirming previous hypotheses [37, 39]. That the ions seem to arrange themselves always in the same configuration, points out to the ions being able to restructure themselves in the gas phase once the solvent is gone. This has been indirectly proven through IMS-IMS studies of entangled chains [50]. Following the disentanglement of two chains mid-drift through ion activation between two IMS stages, the free chains restructure themselves depending on their new charge into configurations that resemble those of single chains with the same amount of charge coming out directly from the solvent. However, under the same ion activation energies, none of the single chain structures were modified. This points out that either gas configurations are extremely stable or "frozen" as described by other groups [77], or that they have the ability to restructure themselves extremely fast in gas the phase to an equilibrium structure (or more than one, as shown in Figure 3c, where multiple structures seem to coexist in transition regions). For a more comprehensive study of collision induced behavior and fragmentation one can refer to recent work by the Pauw's group [78].

Particularities of the PCL Spectra

The contour plot of the PCL ions is strikingly similar to that of PEG with the added difference that the larger monomer mass of the PCL (114 vs 44 Da for PEG) makes ions individually discernible specially for the lower charge states. The high resolution of the DT contour plot, Figure 3c, also allows much higher charge states to be observable. One can easily discern individual ions up to *track* + 17 and charge states up to > + 20. The portion of *tracks* in the *inverse* evolution regions are more spaced out from one another than in PEG to the point where tracks are now fully separated in the first two transitions, T1 and T2. Once again, the *inverse* evolution of T1 is weaker and becomes barely distinguishable from the actual *forward* evolution for the larger charge states. The other three visible *inverse* evolutions work in a similar fashion to PEG which seem to give the contour plot a certain 3D depth. Since more charge states are visible, one can certainly see in this figure that the locus curve joining the maximum mobility for the *inverse* evolutions of each transition tends towards an asymptotic value that seems to be same for all the transitions. One last interesting detail observable in Figure 3c is that there seems to be more than one structural configuration in some of the inverse evolution regions as captured in the inset for *tracks* + 3 and + 4. Given the small variation in mobilities, the structures should be quite similar to each other and could be the result of spurious charging agents contained in the solvents.

The contour plot for PCL in N_2 appearing in Figure 3d follows very similar patterns to that of He. Higher charge states are also present here, although the lower mobility resolution precludes separation for charge states higher than 8, although up to charge state 14 is discernable in some portions as shown in the inset. Similar to the case of PEG, the kinks and transitions seem to happen again at the exact *m*/*z* for both He and N_2, something easily verifiable for charge states + 2 through + 5. What is even more thought-provoking is the fact that the kinks and transitions happen at very similar *m*/*z* and mobilities as those of PEG, albeit smaller *m*/*z*. This is regardless of the fact that the monomer unit mass of PCL is almost 3 times that of PEG. This suggests that the PCL monomer is flexible enough so that it can wrap around the charge in a similar fashion to how 2 to 3 monomers would do in the case of PEG. The beads on a string configuration suggests then that for PCL, the coordination number for every charge would be 3 to 5 instead of 8 to 12 for PEG. This would correspond to 6 to 10 oxygen sites per charge for PCL (with 15 to 25 carbons) and 8 to 12 oxygen sites for PEG (with 16 to 24 carbons).

Particularities of the PDMS Spectra

The PDMS contour plots follow once again similar patterns to PEG and PCL but have unique features due to the difference in monomer size. While the molecular weight of 74 Da of the monomer is between that of PEG and PCL, the pendant methyl groups bonded to the Si atom increase the girth of the polymer chain causing a steric hindrance for the polymer to wrap around the charges. This results in the transitions and kinks occurring

at much longer drift times (larger CCS) for the same electric field than for previous polymers as seen in Figure 3e for He. The transitions and kinks also occur at larger *m*/*z* than previous polymers, and careful conversion shows that the DP necessary to become globular is larger than that for PEG and certainly much larger than that for PCL. This suggests that the cohesive forces per monomer are lower in the case of PDMS. The girth also contributes to more gentle evolutions—*inverse* and *forward*—where the mobility varies very smoothly for a given track for a large range of *m*/*z*. This is particularly visible in the N_2 plot of Figure 3f where mobility is almost constant for tracks 4+ through 10+ from 2000 to 3000 Th (shown in the inset). This has important implications in the study of unfolded proteins as chains of polypeptides would most likely follow gentler evolutions than those produced by PEG or PCL. While there seems to be 3 transitions for *track* + 4 and 2 for *track* + 3, they are difficult to discern. As such, Figure 3f shows a curve joining the center line of the *tracks* with the transitions labeled as T1–T3.

Another outstanding feature of the PDMS contour plots is the existence of cyclic polymers which give rise to a new set of *tracks* (see Figure 3e, f) labeled PDMS-O (also visible in PCL and labeled PCL-O). The fact that they are cyclic can be verified easily through the mass deficiency of the ending groups when compared to their linear counterparts. These tracks differ considerably in mobility from the linear polymer ones (labeled Y-PDMS-X) in the stretched (the chain should be about half the length and double the molecule girth) and transition regions [39, 79]. However, linear and cyclic tracks should eventually merge into one as the ion becomes globular. This can be observed in the PDMS figures from track + 1 to track + 4. Despite this merging, the two tracks may be discernable when sufficient resolution is present in mass and/or mobility. This is visible in Figure 3f for charge state + 1.

Self-Similar Family Shapes in He and N_2 for Polar Polymers

It has been shown previously that the transition configurations for the PEG polymer in N_2 follow well-defined sets of self-similar family shapes that transcend different charge state *tracks* [34, 37, 39, 51]. It will be shown here that these self-similar shapes are not only exclusive to PEG in N_2 but that they also occur for other polymers with a local polar component. Moreover, they are not exclusive to a particular solvent and happen under different pressures and/or gases. From these studies, it can be extrapolated that the self-similar shapes must therefore be only as a result of the potential interaction between charge repulsion and VdW cohesive forces within the gas phase and not as a result of the effect of solvents, buffer gases and/or pressures. In order to show that this is indeed the case, the mobility and *m*/*z* of individual *tracks* for different charge states was obtained from the contourplots by isolating each charge state individually. The crossing/interweaving of the different charge states obstructs this process, as the intensity of a single charge state is falsely enhanced at these intersections (due to the additional intensity of other charge states). Therefore, for each individual *track*, mobility and mass can be well defined for each charge state, meanwhile intensity information is more complicated and will be removed for this process.

Useful structural information can be obtained from using the alternative variables $PA_{s,\,m}$ (projected area) and the CCS, Ω_{gas}, as shown in Figure 5 for PCL and PEG in He and N_2. Ω_{gas} can be inferred from Eq. (3) while the $PA_{s,\,m}$ variable can be obtained from the mass assuming that the ion is to be considered globular and calculating the corresponding projected area as if it were a sphere:

$$PA_{s,m} = \pi \left(\left(\frac{3m}{4\pi\rho_{pol}} \right)^{\frac{1}{3}} + r_g \right)^2, \tag{4}$$

where ρ_{pol} is density of the polymer and r_g is the radius of the gas (considered here to be as an approximation 1. 55 Å for N_2 and 1 Å for He). From theory, in the case of hard sphere elastic specular collisions for a spherical ion: $CCS = PA_{s,\,m}$. Meanwhile, in the case of soft sphere diffuse inelastic collisions, $CCS = \xi PA_{s,\,m}$, where ξ is the accommodation coefficient with values ranging from 1.36 to 1.41 when the ion-induced dipole is considered [80].

Figure 5a, b shows PEG in He and N_2, respectively, while Fig. 5c, d do the same for PCL. In all the figures lines corresponding to $\xi = 1$, 1.25, 1.36, and 1.4 are used for guidance. In general, globular ions should fall between lines with $\xi = 1$–1.4 in this plot [81]. In particular, for N_2, it has been shown that due to diffuse inelastic reemission, this range can be narrowed to $\xi = 1.33$–1.41 for large molecules which is shown to be the case for both polymers [82]. In He, on the other hand, small ions have been shown to have ξ~1 [83–87]. However, as the size of the ion increases, scattering effects increase the value of ξ. This seems to be the case for the polymers presented here where ξ seems to increase with radii from around 1.25 to values slightly below 1.36.

It is expected that ions which are not spherical will fall out of the globular region as clearly shown in Figure 5. It is equally expected that as the ions open up, the effective CCS will be larger than that of a globular ion, $\Omega_{gas} > PA_{s,\,m}$, of the same mass. By choosing one of the *tracks*, one can follow the evolution from spherical to stretched. As the mass of the ion (proportional to $PA_{s,\,m}$) is reduced from the largest globular ion, the ion remains spherical until it eventually reaches a critical mass which leads to the first *inverse* evolution. This inverse evolution is then followed by a *forward* evolution which in Figure 5 shows up as a region with a similar slope to the globular ions. This process -*inverse* and *forward*- is repeated a maximum of *z*-1 times for each charged state as the different transitions (emerging appendices) evolve towards the stretched configuration, leading to the brick-wall system seen in Figure 5. Remarkably, the *forward* evolutions observed for each charge state seem to be continued on other charge states in a similar fashion to what occurs in the globular region. These sets can then be grouped into self-similar families, as observed in Figure 5 by joining the different tracks with a constant line.

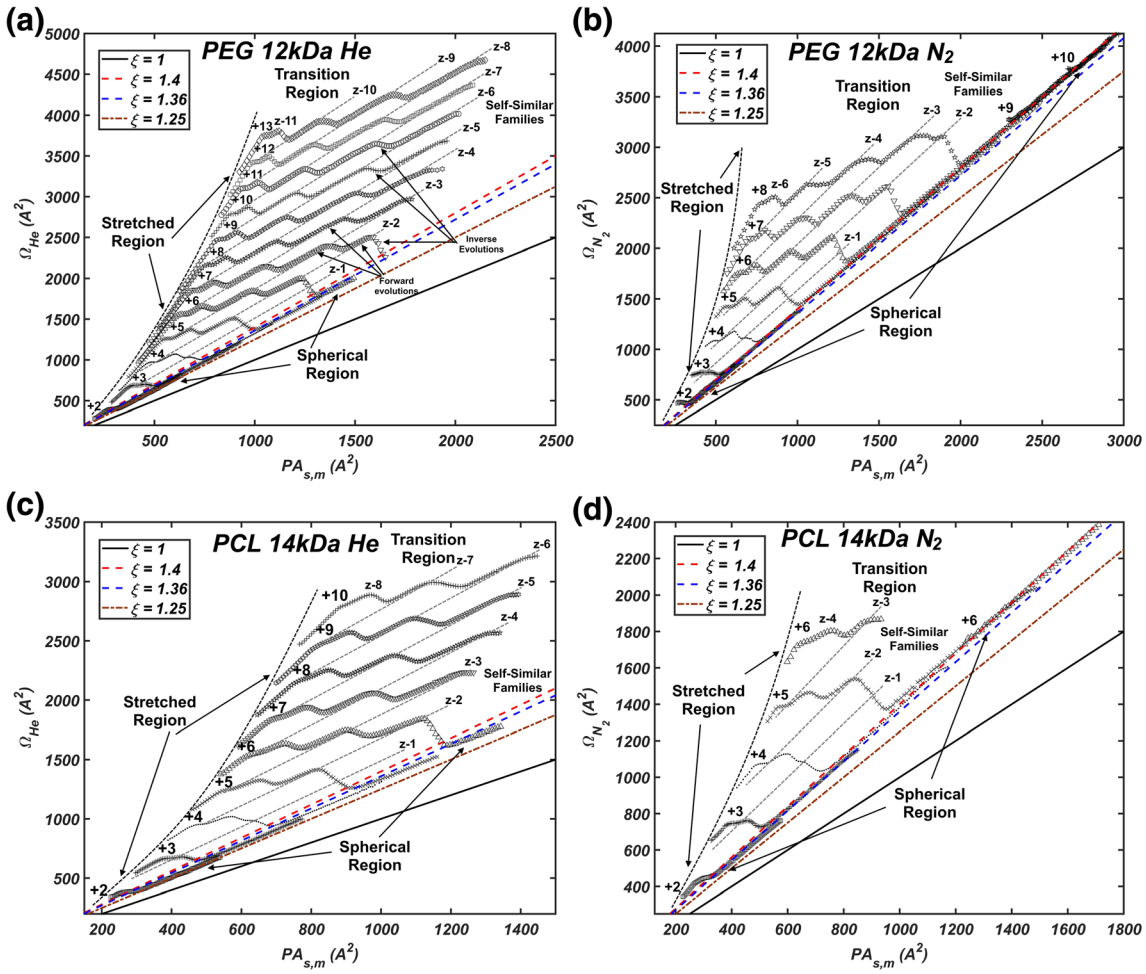

Figure 5. CCS vs. $PA_{s,m}$ for different polymers and gases. (**a**) PEG in He, (**b**) PEG in N_2, (**c**) PCL in He, and (**d**) PCL in N_2. Legend shows the lines corresponding to different accommodation coefficient ξ for a spherical ion of the same density as the polymers

Each of these families have been termed *z-x* where *x* corresponds to the number of charges in the appendix. The fact that self-similar shapes have slopes similar to the globular ions (with mobility resolutions > 150 in the case of He) leads to the reasoning that these ions behave very similar to globules but have an additional drag corresponding to the appendix. Within a self-similar family, the variation of CCS seems to suggest that the length of the appendix remains a quasi-constant addition to the CCS (constant jump in CCS with respect to the spherical ion). This constancy remains true within a given *track* until either the number of monomers in the globule is too small and a new appendix length with a charge protrudes (when traveling through the *track* towards lower masses) or the number of monomers in the globule is sufficient to absorb one of the charges in the appendix (when traveling towards higher masses). The absorption or ejection of the charge happens during the *inverse* evolution portion of the tracks which is visualized in Figure 5 as a strong deviation of the CCS with respect to self-similar families. Finally, although the maximum charge state shown is 13 in the figure, it is clear from the raw data in He of PCL that the families can be extended to charge states higher than 20.

The fact that the same highly resolved evolutions happen within self-similar shapes for all the discernable tracks, for both polymers, for different gases and pressures, and with different solvents used (water vs. toluene) leaves very little doubt to the accuracy of the structural configurations and assumptions here presented. The only plausible doubt that may remain is whether chain extrusion from the droplet does indeed occur under most scenarios presented here. However, that chain extrusion occurs has also been indirectly proven previously through the calculation of the apparent interfacial tension of a globular polymer as the first charge and appendix leaves the globule. The critical mass, m^*, at which this happens for every *track* has been shown to be indirectly proportional to z^2 [34, 37, 39]. This process is reminiscent of the Rayleigh limit of a droplet which relates the maximum charge that a droplet can hold to its surface tension [88]. However, for the known interfacial tension of the polymer, the experimental values disagree with the Rayleigh limit by around 50%. This indicates that perhaps the process of protruding a charge (akin to the Rayleigh limit) occurs at a different critical mass from that of absorbing a charge (for the same number of charges and mass), as in a hysteretical

process, suggesting that the critical mass observed in the contour plots corresponds to that of absorbing a charge, and hence the disagreement. Certainly, the absorption process in the gas phase would only happen if the polymer was indeed ejected from the solvent droplet at least partially unfolded and hence the support of chain extrusion at least partially.

Figure 6 shows the evolution of PDMS in N_2 in the same variables as Figure 5. While the trends should be similar in He, the plot is omitted as only two tracks are complete. Figure 6 is similar in essence to Figure 5 but with notable differences that yield important conclusions. Given that PDMS has methyl pendant groups sticking out of the backbone chain, the self-similar shapes are more difficult to pinpoint, in particular those closer to the spherical region. However, the wavy patterns are still discernible for some of the transitions, especially for higher charge states, and the existence of families is further confirmed through the use of auxiliary dashed lines. The softer variations observed for this polymer may have some important implications regarding the study of gas-phase structures of complex homopolymers and heteropolymers. It is expected that for more complex homopolymers, the transition structures will continue to follow similar trends to the ones predicted here albeit not as clearly defined as with simpler polymers. Single structures for a given mass and charge state seem to be predominant for homopolymers as charges can easily slide from one monomer unit to another. However, this does not seem to be the case for highly charged heteropolymers, e.g., denatured proteins, where multiple structures for the same charge state and mass have been observed [89–94]. The results proposed here can be extrapolated to suggest that these multiple structures will greatly depend on how the hydrophobic and hydrophilic portions of the protein interact with the charges. However, care must be taken when doing these extrapolations as charge locations may be somewhat pre-established in the solvent and may depend on the level of denaturization and strength of the hydrogen bonding. It is clear, anyhow, that with sufficient information, one should be able to provide an accurate description of the tertiary structure in the gas phase and whether or not this structure is related to the native structure present in the solvent.

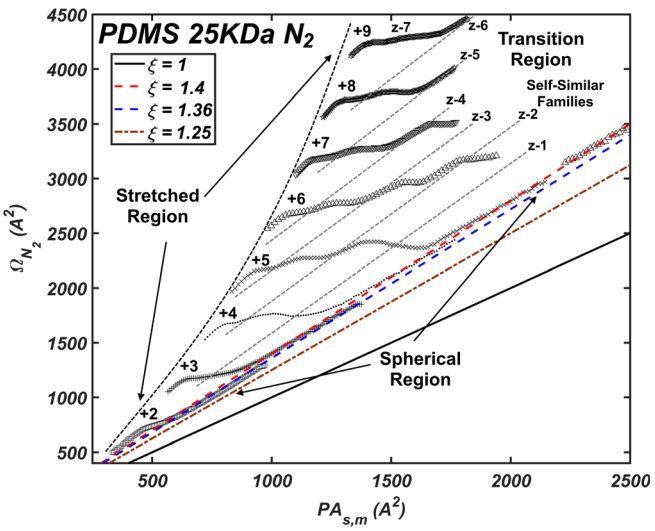

Figure 6. CCS vs. PAs,m for PDMS in N_2. Legend shows the lines corresponding to different accommodation coefficient ξ for a spherical ion of the same density as the polymers

Conclusions

A set of IMS-MS experiments have been undertaken to corroborate the gas-phase structures of homopolymer PEG, and to reveal their similarities with those of PCL and PDMS with two different instruments for different gases—He and N_2—and pressures, atmospheric and low pressure. The following conclusions can be extracted:

1. All the homopolymers studied reveal a sequence of structures in the gas phase that range from stretched to spherical. For these arrangements to happen, the polymers must have an accessible polar covalent bond with a site where the charge can easily attach to. The polymer, as shown previously, then wraps around the charges to form a "beads on a string configuration." The coordination number varies from one polymer to another but does not seem to be related to the mass of the monomer, but to its ability to wrap around the charge.
2. Between the fully stretched and spherical region, a series of transitions are observed for each charge state or *track*. These transitions can be divided into *inverse* and *forward* evolutions, corresponding to either the protrusion of an appendix or the reduction in mass of the main globule respectively.
3. The kinks in the transitions occur at the same *m*/*z* for each polymer regardless of the gas, pressure or system used suggesting that the evolution of these shapes is only dependent on the potential interactions between charges and chain in the gas phase.
4. Moreover, the kinks and transitions for a particular charge state are repeated for all polymers in a similar fashion albeit at different mobilities and masses, suggesting that the structures are also independent, in this case, of the solvent.
5. When CCS is compared between different *tracks* and polymers, self-similar family shapes may be observed for all polymers which transcend charge states. These families are ubiquitous to all polymers and charges leaving little doubt to the description of the structures here encountered.
6. Transitions happen to be smoother for PDMS and this is associated with the larger girth of the chain due to its methyl pendant groups. This is in contrast with what happens with PCL despite its larger monomer size. That only one set structures appear to be predominant for a given mass and charge state for homopolymers may have important implications in the study of more complex heteropolymers in the gas phase.

References

1. Ober, C.K.: Polymer science—shape persistence of synthetic polymers. Science. **288**, 448–449 (2000)

2. Frechet, J.M.J.: Functional polymers and dendrimers—reactivity, molecular architecture, and interfacial energy. Science. **263**, 1710–1715 (1994)
3. Forrest, S.R.: The path to ubiquitous and low-cost organic electronic appliances on plastic. Nature. **428**, 911–918 (2004)
4. Wang, J.Z., Tian, L., Argenti, A., Uhrich, K.E.: Nanoscale amphiphilic star-like macromolecules with carboxy-, methoxy- and amine-terminated chain ends. J. Bioact. Compat. Polym. **21**, 297–313 (2006)
5. Uhrich, K.E., Cannizzaro, S.M., Langer, R.S., Shakesheff, K.M.: Polymeric systems for controlled drug release. Chem. Rev. **99**, 3181–3198 (1999)
6. Aida, T., Meijer, E.W., Stupp, S.I.: Functional supramolecular polymers. Science. **335**, 813–817 (2012)
7. Stupp, S.I., LeBonheur, V., Walker, K., Li, L.S., Huggins, K.E., Keser, M., Amstutz, A.: Supramolecular materials: self-organized nanostructures. Science. **276**, 384–389 (1997)
8. Robinson, B.H.: E-waste: an assessment of global production and environmental impacts. Sci. Total Environ. **408**, 183–191 (2009)
9. Onuchic, J.N., LutheySchulten, Z., Wolynes, P.G.: Theory of protein folding: the energy landscape perspective. Annu. Rev. Phys. Chem. **48**, 545–600 (1997)
10. Hawker, C.J., Wooley, K.L.: The convergence of synthetic organic and polymer chemistries. Science. **309**, 1200–1205 (2005)
11. Mansky, P., Liu, Y., Huang, E., Russell, T.P., Hawker, C.J.: Controlling polymer-surface interactions with random copolymer brushes. Science. **275**, 1458–1460 (1997)
12. Kay, E.R., Leigh, D.A., Zerbetto, F.: Synthetic molecular motors and mechanical machines. Angew. Chem. Int. Ed. **46**, 72–191 (2007)
13. Samori, P.: Scanning probe microscopies beyond imaging. J. Mater. Chem. **14**, 1353–1366 (2004)
14. Mann, S.: Self-assembly and transformation of hybrid nano-objects and nanostructures under equilibrium and non-equilibrium conditions. Nat. Mater. **8**, 781–792 (2009)
15. Howe, D.H., Hart, J.L., McDaniel, R.M., Taheri, M.L., Magenau, A.J.D.: Functionalization-induced self-assembly of block copolymers for nanoparticle synthesis. ACS Macro Lett. **7**, 1503–1508 (2018)
16. Rodriguez-Hernandez, J., Checot, F., Gnanou, Y., Lecommandoux, S.: Toward 'smart' nano-objects by self-assembly of block copolymers in solution. Prog. Polym. Sci. **30**, 691–724 (2005)
17. Hofmann, H., Soranno, A., Borgia, A., Gast, K., Nettels, D., Schuler, B.: Polymer scaling laws of unfolded and intrinsically disordered proteins quantified with single-molecule spectroscopy. P Natl Acad Sci USA. **109**, 16155–16160 (2012)
18. Janshoff, A., Neitzert, M., Oberdorfer, Y., Fuchs, H.: Force spectroscopy of molecular systems - single molecule spectroscopy of polymers and biomolecules. Angew. Chem. Int. Ed. **39**, 3213–3237 (2000)
19. Quake, S.R., Babcock, H., Chu, S.: The dynamics of partially extended single molecules of DNA. Nature. **388**, 151–154 (1997)
20. Wang, M.D., Yin, H., Landick, R., Gelles, J., Block, S.M.: Stretching DNA with optical tweezers. Biophys. J. **72**, 1335–1346 (1997)
21. Fenn, J.B., Mann, M., Meng, C.K., Wong, S.F., Whitehouse, C.M.: Electrospray ionization for mass-spectrometry of large biomolecules. Science. **246**, 64–71 (1989)
22. Tanaka, K., Waki, H., Ido, Y., Akita, S., Yoshida, Y., Yoshida, T., Matsuo, T.J.R.c.i.m.s.: Protein and polymer analyses up to *m/z* 100 000 by laser ionization time-of-flight mass spectrometry. **2**, 151–153 (1988)
23. Costello, C.E.: Time, life ... and mass spectrometry—new techniques to address biological questions. Biophys. Chem. **68**, 173–188 (1997)
24. Clemmer, D.E., Jarrold, M.F.: Ion mobility measurements and their applications to clusters and biomolecules. J. Mass Spectrom. **32**, 577–592 (1997)
25. Armenta, S., Alcala, M., Blanco, M.: A review of recent, unconventional applications of ion mobility spectrometry (IMS). Anal. Chim. Acta. **703**, 114–123 (2011)
26. Nohmi, T., Fenn, J.B.: Electrospray mass-spectrometry of poly(ethylene glycols) with molecular-weights up to 5 million. J. Am. Chem. Soc. **114**, 3241–3246 (1992)
27. Fenn, J.B.: Electrospray wings for molecular elephants (Nobel lecture). Angew. Chem. Int. Ed. **42**, 3871–3894 (2003)
28. Fenn, J.B., Rosell, J., Meng, C.K.: In electrospray ionization, how much pull does an ion need to escape its droplet prison? J. Am. Soc. Mass Spectrom. **8**, 1147–1157 (1997)
29. Wong, S.F., Meng, C.K., Fenn, J.B.: Multiple charging in electrospray ionization of poly(ethylene glycols). J Phys Chem-Us. **92**, 546–550 (1988)
30. Von Helden, G., Wyttenbach, T., Bowers, M.T.: Conformation of macromolecules in the gas-phase - use of matrix-assisted laser-desorption methods in ion chromatography. Science. **267**, 1483–1485 (1995)
31. Wyttenbach, T., von Helden, G., Bowers, M.T.: Conformations of alkali ion cationized polyethers in the gas phase: polyethylene glycol and bis[(benzo-15-crown-5)-15-ylmethyl] pimelate. Int. J. Mass Spectrom. **165**, 377–390 (1997)
32. Von Helden, G., Wyttenbach, T., Bowers, M.T.: Inclusion of a Maldi ion-source in the ion chromatography technique—conformational information on polymer and biomolecular ions. Int. J. Mass Spectrom. **146**, 349–364 (1995)
33. Gidden, J., Wyttenbach, T., Jackson, A.T., Scrivens, J.H., Bowers, M.T.: Gas-phase conformations of synthetic polymers: poly(ethylene glycol), poly(propylene glycol), and poly(tetramethylene glycol). J. Am. Chem. Soc. **122**, 4692–4699 (2000)
34. Ude, S., de la Mora, J.F., Thomson, B.A.: Charge-induced unfolding of multiply charged polyethylene glycol ions. J. Am. Chem. Soc. **126**, 12184–12190 (2004)
35. Trimpin, S., Clemmer, D.E.: Ion mobility spectrometry/mass spectrometry snapshots for assessing the molecular compositions of complex polymeric systems. Anal. Chem. **80**, 9073–9083 (2008)
36. Trimpin, S., Plasencia, M., Isailovic, D., Clemmer, D.E.: Resolving oligomers from fully grown polymers with IMS-MS. Anal. Chem. **79**, 7965–7974 (2007)
37. Larriba, C., de la Mora, J.F.: The gas phase structure of coulombically stretched polyethylene glycol ions. J. Phys. Chem. B. **116**, 593–598 (2012)
38. Larriba, C., Hogan, C.J.: Ion mobilities in diatomic gases: measurement versus prediction with non-specular scattering models. J. Phys. Chem. A. **117**, 3887–3901 (2013)
39. Larriba, C. Ph. D. Dissertation, Yale University, New Haven, CT, (2010)
40. Iribarne, J., Thomson, B.: On the evaporation of small ions from charged droplets. 64, 2287–2294 (1976)
41. Dole, M., Mack, L.L., Hines, R.L., Mobley, R.C., Ferguson, L.D., Alice, M.B.: Molecular beams of macroions. 49, 2240–2249 (1968)
42. Hogan, C.J., de la Mora, J.F.: Tandem ion mobility-mass spectrometry (IMS-MS) study of ion evaporation from ionic liquid-acetonitrile nanodrops. Phys. Chem. Chem. Phys. **11**, 8079–8090 (2009)
43. Ahadi, E., Konermann, L.: Modeling the behavior of coarse-grained polymer chains in charged water droplets: implications for the mechanism of electrospray ionization. J. Phys. Chem. B. **116**, 104–112 (2012)
44. Konermann, L., Ahadi, E., Rodriguez, A.D., Vahidi, S.: Unraveling the mechanism of electrospray ionization. Anal. Chem. **85**, 2–9 (2013)
45. Duez, Q., Metwally, H., Konermann, L.: Electrospray ionization of polypropylene glycol: Rayleigh-charged droplets, competing pathways, and charge state-dependent conformations. Anal. Chem. **90**, 9912–9920 (2018)
46. Chung, J.K., Consta, S.: Release mechanisms of poly(ethylene glycol) macroions from aqueous charged nanodroplets. J. Phys. Chem. B. **116**, 5777–5785 (2012)
47. Consta, S., Chung, J.K.: Charge-induced conformational changes of PEG-(Na-n(+)) in a vacuum and aqueous nanodroplets. J. Phys. Chem. B. **115**, 10447–10455 (2011)
48. Consta, S., Malevanets, A.: Manifestations of charge induced instability in droplets effected by charged macromolecules. Phys. Rev. Lett. **109**, (2012)
49. Consta, S., Malevanets, A.: Classification of the ejection mechanisms of charged macromolecules from liquid droplets. J. Chem. Phys. **138**, (2013)
50. Larriba, C., de la Mora, J.F., Clemmer, D.E.: Electrospray ionization mechanisms for large polyethylene glycol chains studied through tandem ion mobility spectrometry. J. Am. Soc. Mass Spectrom. **25**, 1332–1345 (2014)
51. Haler, J.R.N., Morsa, D., Lecomte, P., Jerome, C., Far, J., De Pauw, E.: Predicting ion mobility-mass spectrometry trends of polymers using the concept of apparent densities. Methods. **144**, 125–133 (2018)
52. Haler, J.R.N., Massonnet, P., Chirot, F., Kune, C., Comby-Zerbino, C., Jordens, J., Honing, M., Mengerink, Y., Far, J., Dugourd, P., De Pauw, E.: Comparison of different ion mobility setups using poly (ethylene oxide) PEO polymers: drift tube, TIMS, and T-wave. J. Am. Soc. Mass Spectrom. **29**, 114–120 (2018)
53. Haler, J.R.N., Far, J., Aqil, A., Claereboudt, J., Tomczyk, N., Giles, K., Jerome, C., De Pauw, E.: Multiple gas-phase conformations of a synthetic linear poly(acrylamide) polymer observed using ion mobility-mass spectrometry. J. Am. Soc. Mass Spectrom. **28**, 2492–2499 (2017)

54. de la Mora, J.F.: Why do GroEL ions exhibit two gas phase conformers? J. Am. Soc. Mass Spectrom. **23**, 2115–2121 (2012)
55. Devine, P.W.A., Fisher, H.C., Calabrese, A.N., Whelan, F., Higazi, D.R., Potts, J.R., Lowe, D.C., Radford, S.E., Ashcroft, A.E.: Investigating the structural compaction of biomolecules upon transition to the gas-phase using ESI-TWIMS-MS. J. Am. Soc. Mass Spectrom. **28**, 1855–1862 (2017)
56. Dickinson, E.R., Jurneczko, E., Pacholarz, K.J., Clarke, D.J., Reeves, M., Ball, K.L., Hupp, T., Campopiano, D., Nikolova, P.V., Barran, P.E.: Insights into the conformations of three structurally diverse proteins: cytochrome c, p53, and MDM2, provided by variable-temperature ion mobility mass spectrometry. Anal. Chem. **87**, 3231–3238 (2015)
57. Hall, Z., Politis, A., Bush, M.F., Smith, L.J., Robinson, C.V.: Charge-state dependent compaction and dissociation of protein complexes: insights from ion mobility and molecular dynamics. J. Am. Chem. Soc. **134**, 3429–3438 (2012)
58. Jhingree, J.R., Bellina, B., Pacholarz, K.J., Barran, P.E.: Charge mediated compaction and rearrangement of gas-phase proteins: a case study considering two proteins at opposing ends of the structure-disorder continuum. J. Am. Soc. Mass Spectrom. **28**, 1450–1461 (2017)
59. Michaelevski, I., Eisenstein, M., Sharon, M.: Gas-phase compaction and unfolding of protein structures. Anal. Chem. **82**, 9484–9491 (2010)
60. Porrini, M., Rosu, F., Rabin, C., Darre, L., Gomez, H., Orozco, M., Gabelica, V.: Compaction of duplex nucleic acids upon native electrospray mass spectrometry. Acs Central Sci. **3**, 454–461 (2017)
61. Flick, T.G., Merenbloom, S.I., Williams, E.R.: Effects of metal ion adduction on the gas-phase conformations of protein ions. J. Am. Soc. Mass Spectrom. **24**, 1654–1662 (2013)
62. Pacholarz, K.J., Peters, S.J., Garlish, R.A., Henry, A.J., Taylor, R.J., Humphreys, D.P., Barran, P.E.: Molecular insights into the thermal stability of mAbs with variable-temperature ion-mobility mass spectrometry. Chembiochem. **17**, 46–51 (2016)
63. Pacholarz, K.J., Porrini, M., Garlish, R.A., Burnley, R.J., Taylor, R.J., Henry, A.J., Barran, P.E.: Dynamics of intact immunoglobulin G explored by drift-tube ion-mobility mass spectrometry and molecular modeling. Angew. Chem. Int. Ed. **53**, 7765–7769 (2014)
64. Rus, J., Moro, D., Sillero, J.A., Royuela, J., Casado, A., Estevez-Molinero, F., de la Mora, J.F.: IMS-MS studies based on coupling a differential mobility analyzer (DMA) to commercial API-MS systems. Int. J. Mass Spectrom. **298**, 30–40 (2010)
65. Larriba, C., Hogan, C.J., Attoui, M., Borrajo, R., Garcia, J.F., de la Mora, J.F.: The mobility-volume relationship below 3.0 nm examined by tandem mobility-mass measurement. Aerosol Sci. Technol. **45**, 453–467 (2011)
66. Ude, S., de la Mora, J.F.: Molecular monodisperse mobility and mass standards from electrosprays of tetra-alkyl ammonium halides. J. Aerosol Sci. **36**, 1224–1237 (2005)
67. Amo-Gonzalez, M., Perez, S.: Planar differential mobility analyzer with a resolving power of 110. Anal. Chem. **90**, 6735–6741 (2018)
68. Koeniger, S.L., Merenbloom, S.I., Valentine, S.J., Jarrold, M.F., Udseth, H.R., Smith, R.D., Clemmer, D.E.: An IMS-IMS analogue of MS-MS. Anal. Chem. **78**, 4161–4174 (2006)
69. Merenbloom, S.I., Koeniger, S.L., Valentine, S.J., Plasencia, M.D., Clemmer, D.E.: IMS-IMS and IMS-IMS-IMS/MS for separating peptide and protein fragment ions. Anal. Chem. **78**, 2802–2809 (2006)
70. Hoaglund, C.S., Valentine, S.J., Sporleder, C.R., Reilly, J.P., Clemmer, D.E.: Three-dimensional ion mobility TOFMS analysis of electrosprayed biomolecules. Anal. Chem. **70**, 2236–2242 (1998)
71. Mark, J.E.: Polymer Data Handbook. (2009)
72. Hutmacher, D.W., Schantz, T., Zein, I., Ng, K.W., Teoh, S.H., Tan, K.C.: Mechanical properties and cell cultural response of polycaprolactone scaffolds designed and fabricated via fused deposition modeling. **55**, 203–216 (2001)
73. Bates, O.K.: Thermal conductivity of liquid silicones. 41, 1966–1968 (1949)
74. Mason, E.A.: McDaniel. E.W. John Wiley & Sons, New York (1988)
75. Criado-Hidalgo, E., Fernandez-Garcia, J., de la Mora, J.F.: Mass and charge distribution analysis in negative electrosprays of large polyethylene glycol chains by ion mobility mass spectrometry. Anal. Chem. **85**, 2710–2716 (2013)
76. Consta, S., Oh, M.I., Malevanets, A.: New mechanisms of macroion-induced disintegration of charged droplets. Chem. Phys. Lett. **663**, 1–12 (2016)
77. Duez, Q., Josse, T., Lemaur, V., Chirot, F., Choi, C.M., Dubois, P., Dugourd, P., Cornil, J., Gerbaux, P., De Winter, J.: Correlation between the shape of the ion mobility signals and the stepwise folding process of polylactide ions. J. Mass Spectrom. **52**, 133–138 (2017)
78. Haler, J.R.N., Massonnet, P., Far, J., de la Rosa, V.R., Lecomte, P., Hoogenboom, R., Jérôme, C., De Pauw, E.: Gas-phase dynamics of collision induced unfolding, collision induced dissociation, and electron transfer dissociation-activated polymer ions. (2018)
79. Hoskins, J.N., Trimpin, S., Grayson, S.M.: Architectural differentiation of linear and cyclic polymeric isomers by ion mobility spectrometry-mass spectrometry. Macromolecules. **44**, 6915–6918 (2011)
80. Larriba, C., Hogan, C.J.: Free molecular collision cross section calculation methods for nanoparticles and complex ions with energy accommodation. J. Comput. Phys. **251**, 344–363 (2013)
81. Epstein, P.S.: On the resistance experienced by spheres in their motion through gases. Phys. Rev. **23**, 710 (1924)
82. Millikan, R.A.: The general law of fall of a small spherical body through a gas, and its bearing upon the nature of molecular reflection from surfaces. Phys. Rev. **22**, 1–23 (1923)
83. Campuzano, I.D.G., Larriba, C., Bagal, D., Schnier, P.D.: Ion mobility and mass spectrometry measurements of the humanized IgGk NIST monoclonal antibody. ACS Symp. Ser. **1202**, 75–112 (2015)
84. Shrivastav, V., Nahin, M., Hogan, C.J., Larriba-Andaluz, C.: Benchmark comparison for a multi-processing ion mobility calculator in the free molecular regime. J Am Soc Mass Spectr. 1–12 (2017)
85. Wyttenbach, T., von Helden, G., Batka, J.J., Carlat, D., Bowers, M.T.: Effect of the long-range potential on ion mobility measurements. J. Am. Soc. Mass Spectrom. **8**, 275–282 (1997)
86. Shvartsburg, A.A., Jarrold, M.F.: An exact hard-spheres scattering model for the mobilities of polyatomic ions. Chem. Phys. Lett. **261**, 86–91 (1996)
87. Mesleh, M.F., Hunter, J.M., Shvartsburg, A.A., Schatz, G.C., Jarrold, M.F.: Structural information from ion mobility measurements: effects of the long-range potential. J Phys Chem-Us. **100**, 16082–16086 (1996)
88. Rayleigh, J.W.S.B. Macmillan, (1896)
89. Bush, M.F., Hall, Z., Giles, K., Hoyes, J., Robinson, C.V., Ruotolo, B.T.: Collision cross sections of proteins and their complexes: a calibration framework and database for gas-phase structural biology. Anal. Chem. **82**, 9557–9565 (2010)
90. Jurneczko, E., Barran, P.E.: How useful is ion mobility mass spectrometry for structural biology? The relationship between protein crystal structures and their collision cross sections in the gas phase. **136**, 20–28 (Analyst, 2011)
91. Ruotolo, B.T., Benesch, J.L.P., Sandercock, A.M., Hyung, S.J., Robinson, C.V.: Ion mobility-mass spectrometry analysis of large protein complexes. Nat. Protoc. **3**, 1139–1152 (2008)
92. Breuker, K., McLafferty, F.W.: Stepwise evolution of protein native structure with electrospray into the gas phase, 10(−12) to 10(2) S. P Natl Acad Sci USA. **105**, 18145–18152 (2008)
93. Steinberg, M.Z., Elber, R., McLafferty, F.W., Gerber, R.B., Breuker, K.: Early structural evolution of native cytochrome c after solvent removal. Chembiochem. **9**, 2417–2423 (2008)
94. Breuker, K., Jin, M., Han, X.M., Jiang, H.H., McLafferty, F.W.: Top-down identification and characterization of biomolecules by mass spectrometry. J. Am. Soc. Mass Spectrom. **19**, 1045–1053 (2008)